JOURNAL OF AIRCRAFT
Vol. 41, No. 4, July–August 2004

Compressible Dynamic Stall Control Using a Variable Droop Leading Edge Airfoil

M. S. Chandrasekhara,* P. B. Martin,† and C. Tung‡
NASA Ames Research Center, Moffett Field, California 94035-1000

The control of compressible dynamic stall using a variable droop leading edge airfoil is described. The leading 25% of a VR-12 airfoil is drooped as it executes sinusoidal pitch oscillations such that the leading portion of the airfoil is always at a low effective incidence to the flow. Airfoil performance data determined for freestream Mach numbers ranging from 0.2 to 0.4, at reduced frequencies from 0 to 0.1, and using unsteady pressure transducer measurements, show that droop reduces the tendency of the airfoil to enter the dynamic stall state. Even when it does, the strength of the dynamic stall vortex is significantly reduced, which is reflected in the 40 to 50% smaller negative peak pitching-moment values, with positive damping of the airfoil. Also, the airfoil drag when the droop is dynamically varied is reduced by up to 75% relative to a nondrooped airfoil, making a strong case for the use of this concept for dynamic stall control.

I. Introduction

THE excessive vibratory loads arising from the large pitching-moment variations that accompany the onset of compressible dynamic stall have limited the operational envelope of a helicopter rotor. Consequently, the major benefit of dynamic stall, the dynamic lift, has remained unutilized. This has limited the capabilities of helicopters considerably by preventing them from performing many crucial maneuvers such as nap of the Earth and urban transport. Because the U.S. Army has stipulated that the next generation of rotorcraft be significantly more capable than the existing fleet, it has become imperative that future designs incorporate concepts that exploit the benefits of dynamic stall. Such designs obviously require the use of successful dynamic stall control methods in order to meet the new specifications. The present work takes a step in that direction by evaluating a dynamic stall control concept referred to as the variable droop leading edge (VDLE) airfoil. Owing to the fact that the structural problems associated with dynamic stall are directly attributable to the formation and convection of a strong, coherent dynamic stall vortex, dynamic stall control is defined here as the avoidance or at least a significant reduction of the strongly negative pitching moment arising from the dynamic stall vortex convection, while attempting to retain the inviscid lift up to high angles of attack.

Earlier research (Ref. 1) has shown that the mechanisms responsible for compressible dynamic stall onset change rapidly with flow conditions. However, the common element in all of the known mechanisms is the strong leading edge adverse pressure gradient. This led to the conclusion that dynamic stall control requires control of this pressure gradient. Based on this logic, several compressible dynamic stall control methods have been devised (Ref. 2). In particular, successful control has already been demonstrated up to $M = 0.4$ on a symmetric NACA 0012 airfoil using the dynamically deforming leading edge (DDLE) airfoil concept. In this, the airfoil leading edge curvature was dynamically varied by as much as 320% by retracting its nose a very small (of the order of 1% chord) distance. This produced gross potential flow changes and resulted in a dramatically improved airfoil instantaneous pressure distribution that favorably influenced the dynamic stall vorticity field and enabled control (Ref. 3). Dynamic stall control was also achieved using other methods. In one such approach, a fixed leading edge slat on a cambered airfoil (slatted airfoil) was used to control compressible dynamic stall at Mach numbers of up to 0.4 (Ref. 4). In this study, different leading edge slats were shown to be effective in preventing the formation of the dynamic stall vortex on the main element of the airfoil to different extents. The natural bleed flow through the slat-airfoil slot was found to be sufficient to produce the desired effects.

Although both the DDLE airfoil and the slatted airfoils were proven to be successful in achieving dynamic stall control, the need to maintain a highly flexible leading edge surface (from concerns of leading edge erosion, strength and blade rigidity) in the former and the permanent drag of the slat on the rotor advancing side with the latter approach was deemed somewhat restrictive. In an attempt to overcome these limitations, the VDLE airfoil was conceived. A similar concept had shown promise earlier in the U.S. Army tests in a water tunnel and in incompressible flow computations (Ref. 5). The airfoil under consideration is the cambered VR-12 airfoil, which is representative of rotorcraft airfoils and has excellent performance for the advancing side flow conditions. Conceptually, a portion of the retreating blade leading edge is drooped dynamically, so that it is at a reduced incidence to the oncoming stream. Because dynamic stall is a leading edge phenomenon arising from a number of different flow mechanisms for small changes in flow conditions (Ref. 1), this approach offered a way to modify the local adverse flow effects suitably to improve the airfoil performance on the retreating side.

To maintain robust control of dynamic stall, several parameters must be considered. In particular, it is recognized here that the control problem is one of unsteady vorticity production and its management involving two independent flow timescales: the airfoil reduced frequency through which it is produced and the rate of change of airfoil droop through which its diffusion and convection (i.e., vorticity management) are controlled. These two flow scales can interact with each other during an airfoil oscillation cycle. Just as was discovered with the DDLE airfoil, it is possible to create either a favorable interaction by a proper selection of the droop rates involved relative to the airfoil oscillation to achieve successful control or an unfavorable one to induce premature dynamic stall onset by a mismatch. Hence, the study initially focused on the effects of various fixed values of leading edge droop angle and then on some possible droop

Presented as Paper 2003-0048 at the 41st Aerospace Sciences Meeting and Exhibit, Reno, NV, 6 January 2003; received 13 January 2003; revision received 16 May 2003; accepted for publication 26 May 2003.

*Research Professor and Acting Director, Department of Mechanical Engineering and Astronautics, NASA Ames Research Center, M.S. 215-1, Moffett Field, California 94035-1000. Associate Fellow AIAA.

†Research Scientist, U.S. Army Aeroflightdynamics Directorate, AMCOM. Member AIAA.

‡Deputy Branch Chief, U.S. Army Aeroflightdynamics Directorate, AMCOM, M.S. T12-B. Member AIAA.

variations, within the possibilities provided by the drive mechanisms. During this first phase of the study, emphasis was placed on deriving the performance characteristics of the various airfoil geometries that resulted. Future efforts will also consider the underlying fundamental fluid dynamic aspects.

The study consisted of first designing an instrumented VR-12 airfoil with its leading 25% drooping as desired. It was subsequently tested in the compressible dynamic stall facility (CDSF). Airfoil pressures as well as point diffraction interferometry data were acquired for each system setting for various flow conditions from which the airfoil performance was quantified. A description of the effort follows along with the results obtained.

II. Description of the Experiment

The tests were conducted at Mach numbers ranging from 0.2 to 0.4 and at reduced frequencies from 0 to 0.1 in the NASA Ames Research Center Fluid Mechanics Laboratory 25×35 cm compressible dynamic stall facility. The uniqueness of the CDSF is that an airfoil is mounted between its sidewalls and oscillated as $\alpha(t) = \alpha_m - \alpha_a \sin \omega t$, where α_m is the mean angle of attack, $0 \text{ deg} < \alpha_m < 15$ deg, and α_a is the amplitude of oscillation, $2 \text{ deg} < \alpha_a < 10$ deg. A specially designed oscillation mechanism mounted at the top enables oscillating the airfoil up to 100 Hz. Reference 6 provides a complete description of the CDSF and its instrumentation.

A. Variable Droop Leading Edge Airfoil

Figure 1 shows the VDLE airfoil in two configurations, a basic VR-12 airfoil and a fixed-droop VR-12 airfoil. Figure 2 presents the model assembly. The model has a 15.2-cm chord and a span of 25 cm. It is built in two parts, the drooping front 25% and the main element; the two are connected through a hinge at the quarter-chord point (see Fig. 2). The main element has machined rectangular tangs that are used to hold it in matching slots in the CDSF windows that oscillate about the quarter-chord point. Thus, the main element oscillates synchronously with the windows. The drooping portion of the airfoil is fully supported by the hinge. The hinge shaft is hollow (for carrying instrumentation leads) and protrudes out of the CDSF windows. It is connected to drive linkages (see Fig. 2) on either side of the test section. If these linkages are anchored to the oscillating windows, a fixed leading edge droop angle results through the oscillation cycle. Moving the location of the anchor point on the oscillating windows changes the droop. A continuously variable droop results if the anchor point is fixed to the tunnel sidewalls. The

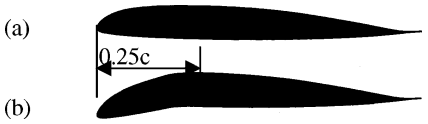

Fig. 1 Original VR-12 compared with the VR-12 VDLE profile.

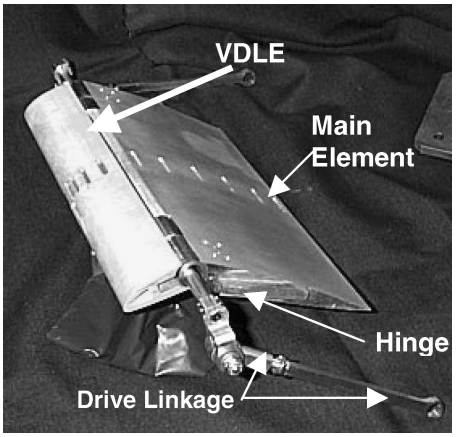

Fig. 2 Assembled VDLE airfoil.

Table 1 Locations of the pressure taps on the VDLE airfoil

	x/c	
No	Upper surface	Lower surface
1	0.00	0.01
2	0.01	0.025
3	0.025	0.05
4	0.05	0.15
5	0.10	0.30
6	0.175	0.50
7	0.275	0.70
8	0.40	0.90
9	0.55	——
10	0.70	——
11	0.85	——
12	0.95	——

droop value varies as

$$\delta_{\text{instantaneous}} = \alpha - \delta_{\text{initial}}$$

In the variable droop mode of operation, the leading edge remains at a fixed orientation in the laboratory coordinate system, but the main element changes its incidence through the oscillation cycle. The maximum permissible droop angle is 25 deg, which provides a maximum initial droop angle of -5 deg for the case of angle of attack varying as $\alpha = 10 \text{ deg} + 10 \text{ deg} \sin \omega t$. To vary the droop in an arbitrary manner, a low-mass drive system connected to the oscillating windows to control the airfoil droop independently of the amplitude of oscillation is under consideration.

B. Instrumentation and Technique

The model was instrumented with 20 flush-mounted, sealed gauge, Kulite unsteady, absolute pressure transducers at locations listed in Table 1, with 10 transducers in the drooping front portion and the rest in the main element on both upper and lower surfaces. The power supply and signal leads from these transducers were drawn between the model surfaces, and they exit the model from the hollow hinge shaft at the quarter-chord point. The transducers were individually connected to a 15-V dc power supply and signal conditioners. The conditioned analog signal from each unit was recorded with a high-speed (Microstar Laboratories) analog digital converter (ADC) simultaneously with a digital encoder signal that provided the airfoil instantaneous angle-of-attack information using custom developed LabVIEW software. Typical sampling rates used were 4 KHz/channel with 40,000 samples/channel. At the oscillation frequencies used (up to 30 Hz), a sufficiently large number of realizations occurred with this approach. The data were ensemble averaged after randomly initiating the acquisition and later sorting it into 800 bins, each one encoder-count wide (corresponding to angle of attack bins of 0.002 to 0.08 deg depending on the phase angle through the sine wave of oscillation cycle for $\alpha = 10$ deg $+10$ deg $\sin \omega t$). Anywhere from 40 to 100 samples were present in each bin. The standard deviation of the data was generally low (less than 3%), which resulted in a low uncertainty of the measured ensemble-averaged unsteady pressures. The transducers also have excellent temperature stability specifications.The transducers were calibrated individually by enclosing them in a suitable suction cup that was evacuated using an ISO 9000 certified Mensor pressure calibration unit over the anticipated range of pressures. The CDSF is an in-draft wind tunnel drawing air from the atmosphere and discharging into an evacuation compressor. Thus, the maximum pressure anywhere in the flow was atmospheric, with only suction at all locations over the airfoil. All 20 transducers were found to be linear over the range tested. Because absolute pressures were measured, considerable care was taken during calibration and experimentation to account for changes in ambient pressure (caused by weather front movements), noise, drift, and such extraneous factors. The wind-tunnel stagnation pressure, the static pressure, and the dynamic pressure were measured using a Setra differential pressure transducer, with a verification of the ambient pressure from the

Mensor calibration unit. Thus, it was possible to account for any drifts or environmental effects.

Quantitative flow visualization was conducted using the real-time technique of point diffraction interferometry (PDI). Details of the PDI technique are provided in Ref. 7. Several interferograms were acquired for each flow condition. Although PDI is a quantitative technique, the interferograms will be used here only for their qualitative value because the field of view was limited to $-0.2 < x/c < 0.4$ and the pressure data are available over the whole airfoil.

C. Calculation of C_l, C_d, and C_m

As stated earlier, the measured instantaneous voltages were sorted into 800 bins prior to saving the data. The contents of these bins were converted to pressures using the calibrations for the respective transducers; the mean and standard deviations of the data set were computed for the pressure coefficient. The lift, drag, and pitching-moment coefficients were calculated for each bin from the normal and axial forces computed by integrating the pressure coefficients, knowing the sensor spacing and the airfoil instantaneous geometry. For the fixed-droop case, the transducer locations were transformed along the main element chord line, as is standard practice in high-lift device aerodynamics. For the VDLE case, the transformation was carried out for each instantaneous angle of attack.

D. Experimental Conditions

The experimental data were obtained for the following: Mach number M, 0.2, 0.3, and 0.4; reduced frequency, ≈ 0 (quasi steady); $k = \pi f c/U_\infty$, 0.025, 0.05, 0.075, and 0.1; droop angle δ, 0, 5, 10, 15, 20 deg for the VDLE case $\delta_{\text{initial}} = 0$ deg (at $\alpha = 0$ deg); angle of attack $\alpha(t)$, $10 - 10 \deg \sin \omega t$; and Reynolds number Re, 0.7×10^6–1.6×10^6.

The steady flow data actually correspond to a slow oscillation of the airfoil at $k \approx 0.002$.

E. Measurement Uncertainty

The following uncertainties have been estimated for the various quantities: Mach number, ± 0.005; angle of attack, 0.05 deg; reduced frequency, 0.005, C_p, ± 0.05 at $M = 0.3$; and C_l, C_d, and C_m are 0.05, 0.05, and 0.005.

III. Results and Discussion

A large experimental database has been generated from the wind-tunnel studies. In the following, some key results will be presented and discussed to demonstrate the effects of and the need for drooping the leading edge of an airfoil as a means of compressible dynamic stall control.

A. Point Diffraction Interferograms at $M = 0.3$ and 0.4

Figure 3 compares the flow density fields as seen from the point diffraction interferograms at $M = 0.3$, $k = 0.1$ at different angle of attack for the basic VR-12 airfoil (Figs. 3a and 3b) and for the case of $\delta = 10$ deg (Figs. 3c and 3d). It can be seen from Fig. 3a that for the basic (no-droop) airfoil, at the high angle of $\alpha = 17$ deg, the flow has become supersonic around the leading edge and weak shocks form. However, these do not cause any noteworthy flow separation. For this condition, the dynamic stall appears to be just beginning with trailing-edge flow reversal propagating towards the leading edge. By $\alpha = 20$ deg, Fig. 3b, the process is complete and has moved to the leading edge, with a well-defined dynamic stall vortex and a secondary vortex also visible in the image. The large number of fringes visible in the image before the stall onset point suggests that the dynamic stall seen here is largely pressure gradient induced, even though there was mild supersonic flow in the leading edge region. The pressure distributions to be discussed later support this inference.

When droop is added to the leading edge region, the flow behavior changes considerably. At $\alpha = 17$ deg, Fig. 3c, the airfoil peak suction is still significantly less than what was observed for the no-droop case. This is inferred from the number of fringes present around the leading edge (greater the number, higher the suction pressure coefficient). The flow remains attached to a greater extent over the upper surface, with a only slight flow distortion seen near $x/c = 0.25$ as a result of the mild backward-facing step that forms along the hinge line. The leading section of the airfoil is effectively at a lower incidence to the flow and thus does not stall even at this high angle of attack. It also develops less suction, but because compressible dynamic stall is a leading edge type of stall it effectively permits dynamic stall control. It is clear that drooping the airfoil provides a definite benefit at high angles of attack. Figure 3d shows that even at $\alpha = 20$ deg there is fully attached leading edge flow; only trailing-edge separation, and no dominant dynamic stall vortex can be detected in the visible portion of the flow.

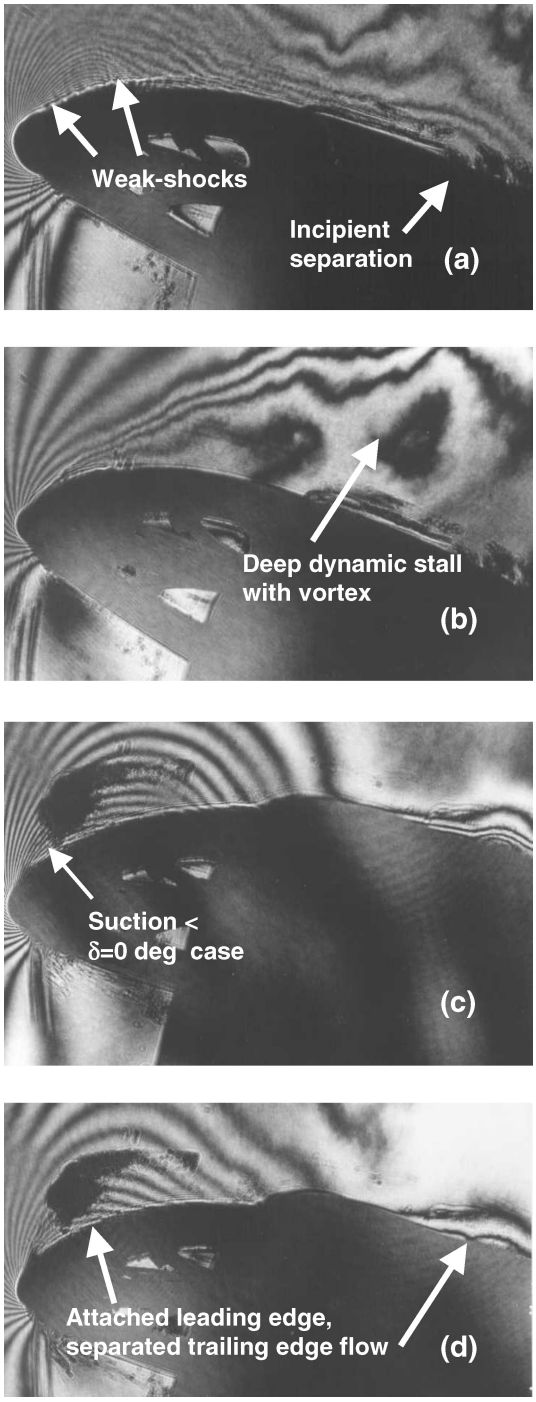

Fig. 3 Comparison of PDI images for $M = 0.3$, $k = 0.1$: a) $\alpha = 17$ deg, $\delta = 0$ deg; b) $\alpha = 20$ deg, $\delta = 0$ deg; c) $\alpha = 17$ deg, $\delta = 10$ deg; and d) $\alpha = 20$ deg, $\delta = 10$ deg.

For $M = 0.4$, the flow becomes strongly supersonic at $k = 0.1$, and shock-induced separation occurs as shown in Fig. 4a at $\alpha \approx 14$ deg. It is thus clear that the flow nature has changed dramatically for this 0 deg-droop case as the Mach number is increased from $M = 0.3$ to 0.4. A simple fringe count indicates that the local Mach number is very high (>1.2) and strong enough to cause shock-induced separation (Ref. 4). Until the vortex convects downstream, the airfoil peak suction increases; subsequently, it falls. At $\alpha = 20$ deg, the flow has completely stalled, as can be seen in Fig. 4b. Once again, the pressure distributions shown later confirm the result seen here. In contrast, for the 10-deg-droop airfoil flow, there is no supersonic flow that develops at either $\alpha = 14$ deg (Fig. 4c) or at $\alpha = 20$ deg (Fig. 4d). The leading edge flow remains fully subsonic always. For the latter case, trailing-edge separation is seen to progress towards the leading edge as was seen for $M = 0.3$. What is even more interesting here is the fact that adding droop has completely altered the flow behavior, the mechanism of dynamic stall, and the stall process in general over this airfoil. For both $M = 0.3$ and $M = 0.4$, no dynamic stall vortex can be seen in these images. Thus, it can be concluded that stall control was achieved by altering the fundamental physical processes involved in the flow.

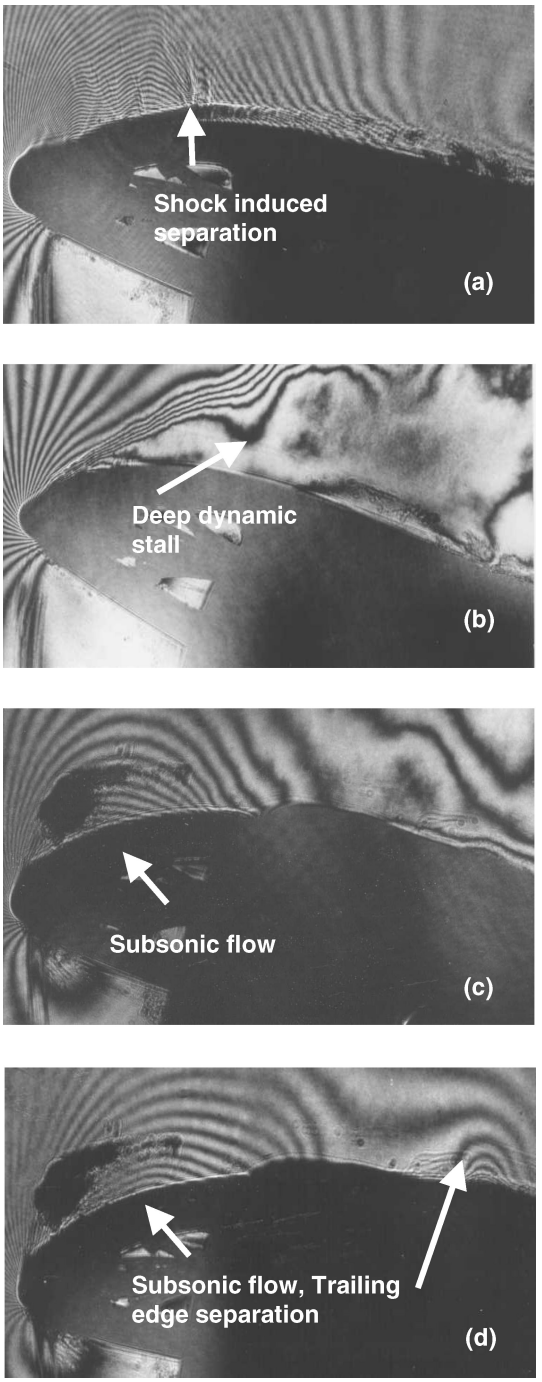

Fig. 4 Comparison of PDI images for $M = 0.4$, $k = 0.1$: a) $\alpha = 14$ deg, $\delta = 0$ deg; b) $\alpha = 20$ deg, $\delta = 0$ deg; c) $\alpha = 14$ deg, $\delta = 10$ deg; and d) $\alpha = 20$ deg, $\delta = 10$ deg.

B. Airfoil Pressure Distributions

Figure 5 compares the surface-pressure distributions for the basic VR-12 and the VDLE airfoils at $M = 0.3$, $k = 0.1$. (Note that the lower surface is represented by negative values of x/c with $x/c = -1.0$ at the trailing edge.) The peak suction over the basic airfoil rises steeply with angle of attack, and the pressure coefficient attains a very high value of -7.92, which is in excess of the critical pressure coefficient for this Mach number. Thus, shocks can form in the flow, which were seen in Fig. 3a. However, as the PDI pictures revealed, the shocks are weak and do not induce flow separation. For this test condition, the adverse pressure gradient following the suction peak is significant, leading to dynamic stall. The passage of the dynamic stall vortex is clearly seen in the pressure distributions as a gradually rising pressure with increasing α, corresponding to the vortex center, following the loss of the suction peak. An interesting feature that is noticed here is that the vortex has not convected past the airfoil trailing edge at $\alpha = 20$ deg. This can be deduced from the result that the pressure coefficient at the trailing edge has not fallen to zero at $\alpha = 20$ deg, indicating that the vortex formed late in the upstroke. It appears to be shed during the airfoil downstroke.

In contrast, the VDLE airfoil pressure distributions in Fig. 5b show that the peak suction values are considerably lower (-3.46). Thus, the adverse pressure gradient downstream is also lower. In general, the suction values appear to lag the basic airfoil pressures in angle of attack and magnitude because of the drooping effect. The

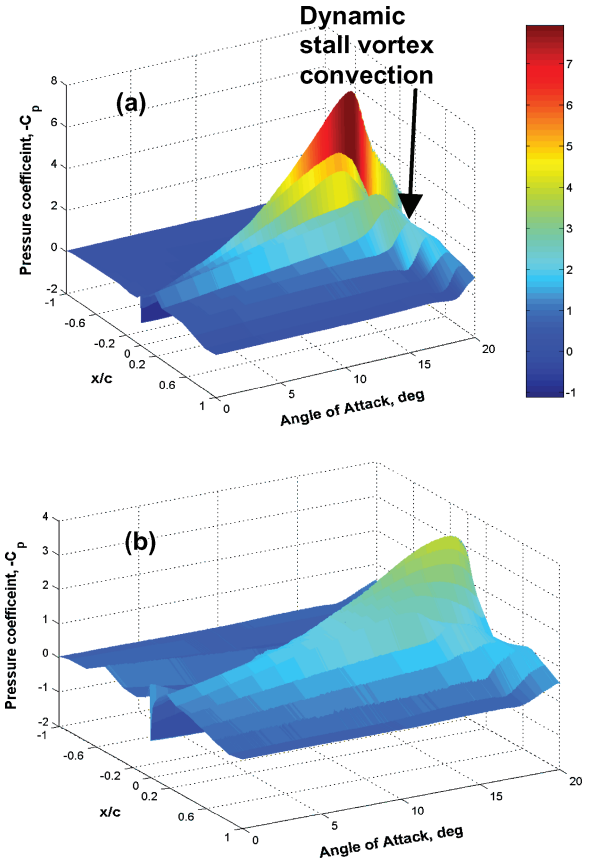

Fig. 5 Comparison of upper-surface-pressure distributions; $M = 0.3$, $k = 0.1$: a) basic VR-12 airfoil, and b) variable droop leading edge airfoil.

flatter pressure distribution seen implies that a reasonably high lift is still produced. The distributions seem to point to the formation of a weak dynamic stall vortex even in this case but, at an even higher angle of attack than was seen in Fig. 5a. Its onset point appears to be downstream of the hinge line, and it still remains on the surface at $\alpha = 20$ deg. Thus, variably drooping the leading edge has delayed onset of dynamic stall. Furthermore, as the onset point is downstream of the aerodynamic center, it can be expected to mitigate the normal adverse effect on the pitching-moment distributions (to be discussed later).

At $M = 0.4$, $k = 0.1$, the basic VR-12 airfoil produces a peak suction-pressure coefficient of about –5.86 (see Fig. 6a), and for the VDLE airfoil the corresponding value is -3.53 (Fig. 6b). The large $C_{p\,\min}$ in Fig. 6a also causes a strong shock to form, which induces separation immediately, and a dynamic stall vortex forms. This convects towards the trailing edge as before. The drop in pressure near the trailing edge indicates that the vortex has convected past $x/c = 1.0$ by $\alpha = 20$ deg. As has been seen in compressible dynamic stall studies over an NACA 0012 airfoil (Ref. 1), the surface signature of the vortex when induced by a shock is flatter than when it is induced by just the pressure gradient. These characteristics are completely suppressed because of drooping in the VDLE airfoil flow. The pressure distributions look akin to that at $M = 0.3$, thereby pointing to the fact that the VDLE concept has an additional advantage of largely mitigating the strong compressibility effects, enabling a better performance to be attained from the same airfoil at higher Mach numbers. The gradual fall of the suction peak pressure and the semblance of a vortex forming aft over the upper surface once again suggest that the pitching-moment variations are likely to be favorable in the VDLE case even at $M = 0.4$.

C. Effect of Droop on Performance Parameters

The lift, drag, and pitching-moment coefficients of the various resulting airfoils were calculated as described earlier. Figure 7 presents some results, wherein C_l is plotted as a function of the angle of attack for $M = 0.3$, $k = 0.1$ for $0 \le \delta \le 20$ deg. The basic VR-12 airfoil performs as expected with a $C_{l_{\max}}$ of about 1.8 at $\alpha = 16$ deg before dynamic stall onset. The lift drops rapidly near $\alpha = 20$ deg, and a large hysteresis is evident. It appears that flow reattachment is not complete until very low angles of attack. With increasing droop angles, the C_{l_0} value progressively decreases as does the $C_{l_{\max}}$. However, the VDLE airfoil shows a gradual loss of lift compared to all fixed-droop cases studied indicating a softer stall behavior.

In Fig. 8, the lift coefficient for the VDLE airfoil is plotted for different reduced frequencies, $0 \le k \le 0.1$. The progressive increase in $C_{l_{\max}}$ with k is evident. It appears that for the quasi-steady case and $k = 0.025$ cases the stall onset angle is sufficiently below the maximum angle of attack (of 20 deg) so that the two exhibit an unusual poststall lift behavior. For higher values of k, once again, the expected trailing-edge type of poststall lift behavior is seen. Also, the hysteresis loop becomes wider with increasing frequency, and on the downstroke the linear C_l vs α behavior for $k = 0.1$ is

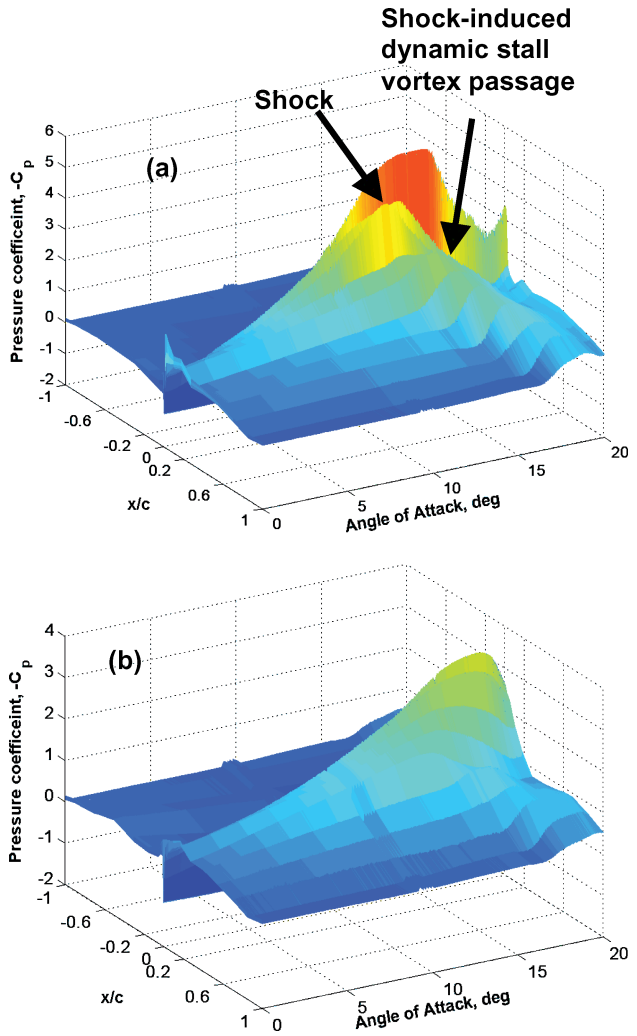

Fig. 6 Comparison of upper-surface-pressure distributions; $M = 0.4$, $k = 0.1$: a) basic VR-12 airfoil, and b) variable droop leading edge airfoil.

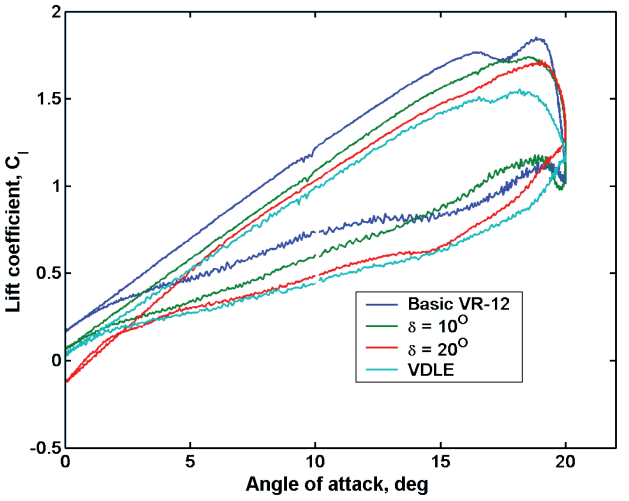

Fig. 7 Effect of droop on lift coefficient: $M = 0.3$, $k = 0.1$, and $\alpha = 10$ deg +10 deg sin ωt.

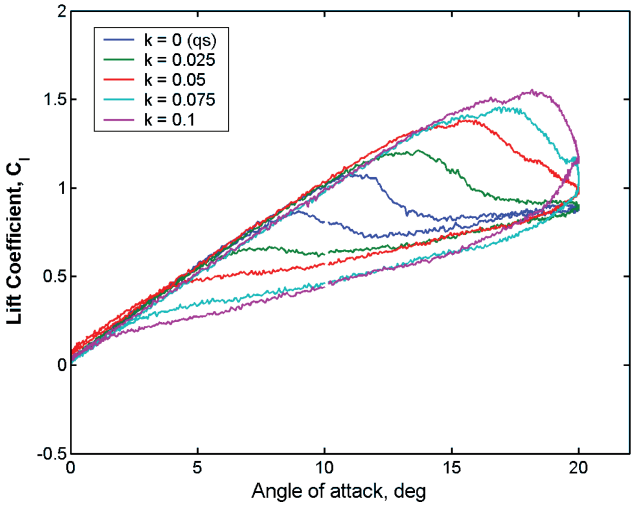

Fig. 8 Effect of reduced frequency on lift coefficient: VDLE airfoil, $M = 0.3$, and $\alpha = 10$ deg +10 deg sin ωt.

limited to angles below $\alpha = 2$ deg, attributable to a delay in complete flow reattachment. Part of the reason for this is believed to be the progressive delay in dynamic stall onset and its continuation into the downstroke. Thus, notable delay effects, which cannot be foreseen, are introduced in the flow.

Figure 9 compares the lift curves for $M = 0.4$ at $k = 0.05$ and 0.1 for the basic VR-12 and the VDLE cases. For both the basic airfoil and the VDLE airfoil, $C_{l_{\max}}$ increases with k, but the value for the basic case is higher than that for the VDLE case as can be expected. However, the dynamic stall angle is slightly delayed for the VDLE cases. For the basic airfoil, the reattachment angle of attack appears to be insensitive to k, but for the VDLE airfoil this is not the case. In fact, at $k = 0.1$ the reattachment angle is later in the downstroke as seen by the fact that the C_l is only linear below $\alpha \approx 1.5$ deg, which indicates a very large hysteresis effect. Also, the stall is more gradual in the VDLE cases.

Figures 10 and 11 show the wind axis drag distributions for the case of $M = 0.3$ and $k = 0.1$. It is well known that a drooping front element on an airfoil is a source of drag. This is clearly seen in Fig. 10, where the C_d value at $\alpha = 0$ deg increases monotonically with droop angle.

For the VDLE airfoil, however, the value at $\alpha = 0$ is slightly higher than that seen for the basic VR-12 case. It appears that the hysteresis effect seen in the lift behavior, which arises from the delayed flow reattachment, is responsible for this small difference. The drag rise angle of attack increases with droop angle, and also the maximum C_d value decreases, with the best performance seen for the VDLE airfoil. The most striking result is that this is true even when a dynamic stall vortex is present. For the VDLE case shown in Fig. 10, the maximum drag coefficient is about 25% of the basic VR-12 case. Thus, a sizeable, 75% drag reduction has been observed in this, and it can be easily deduced that because the lift coefficients are only marginally different the lift-to-drag ratio (L/D) values will be significantly better when droop is used. It is also worth pointing out that the maximum C_d value measured for the VDLE case is even smaller than that measured for the case of fixed 20-deg-droop case, with the value at $\alpha = 0$ deg far more favorable as just stated.

Figure 11 shows that the drag performance of the VDLE airfoil is virtually independent of the reduced frequency, an extremely interesting result because the lift coefficients were substantially different. Thus, one can expect an even better L/D performance from a VDLE airfoil as the reduced frequency is increased.

Drooping the airfoil leading edge reduces the high angle-of-attack drag by a large amount, and only increases the low angle of attack slightly. A VDLE airfoil has nearly the same drag as a basic VR-12 airfoil at low angles and the lowest drag coefficient at high angles of attack, thus making it preferable for the dynamic stall application. Thus, these results strongly support the use of the variably drooping leading edge airfoil because a helicopter rotor operates at virtually zero or even negative angles on the advancing side, making a fixed droop or a slatted airfoil highly undesirable.

Figure 12 compares the drag coefficient for the basic airfoil and the VDLE airfoil at $M = 0.4$ for $k = 0.05$ and 0.1. The maximum drag value appears at a higher angle of attack for both the VDLE cases shown relative to the basic airfoil. Thus, use of the VDLE airfoil enables better operation to higher angles because lift stall is

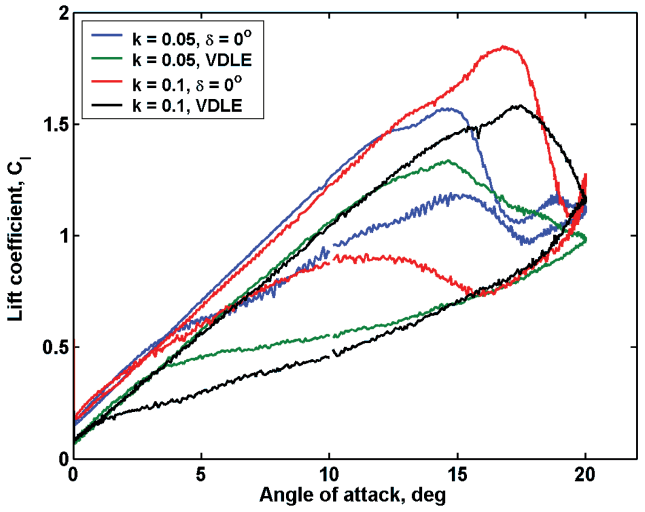

Fig. 9 Effect of variably drooping the leading edge on C_l: $M = 0.4$, and $\alpha = 10$ deg +10 deg sin ωt.

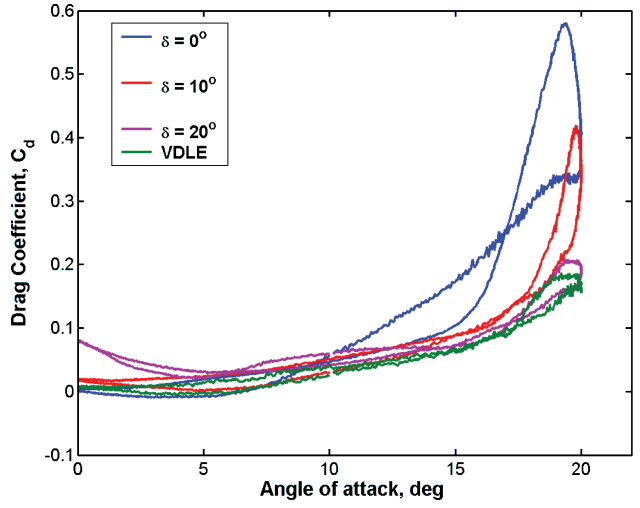

Fig. 10 Effect of droop on drag coefficient: $M = 0.3$, $k = 0.1$, and $\alpha = 10$ deg +10 deg sin ωt.

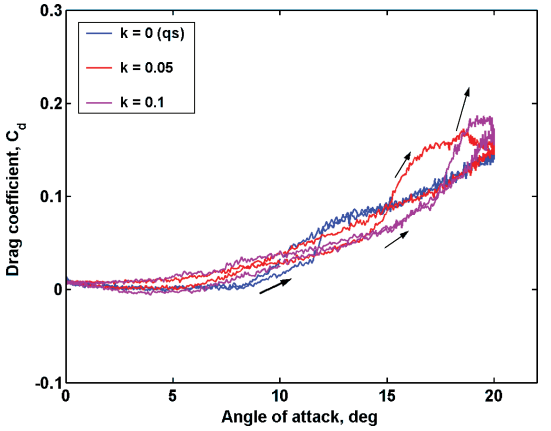

Fig. 11 Effect of reduced frequency on drag coefficient for the VDLE airfoil, $M = 0.3$, and $\alpha = 10$ deg +10 deg sin ωt.

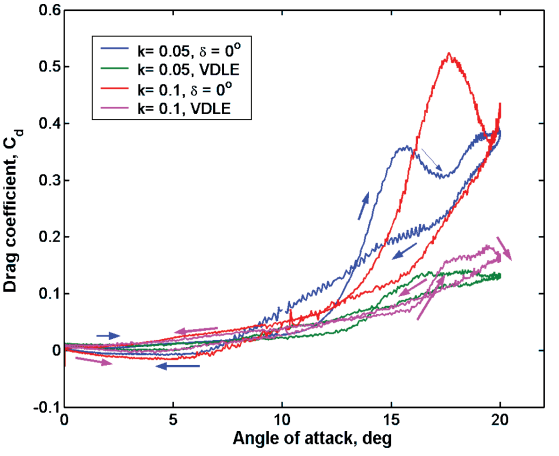

Fig. 12 Comparison of drag coefficient of the basic VR-12 airfoil and the VDLE airfoil: $M = 0.4$, and $\alpha = 10$ deg +10 deg sin ωt.

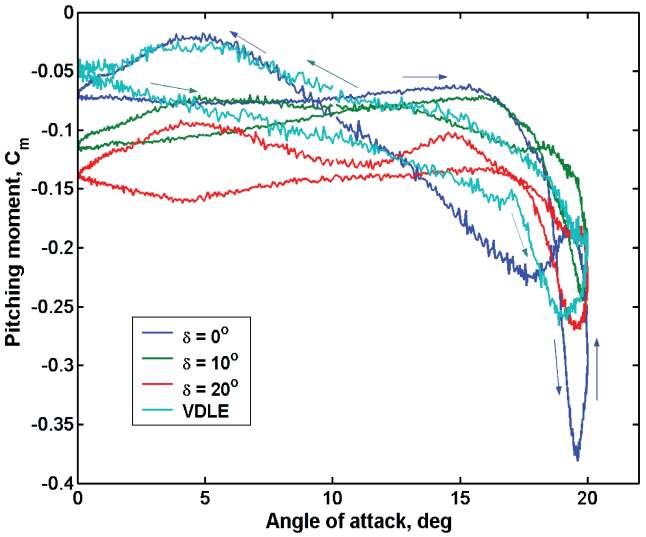

Fig. 13 Effect of droop angle on pitching-moment coefficient for the VR-12 airfoil: $M = 0.3$, $k = 0.1$, and $\alpha = 10$ deg +10 deg sin ωt.

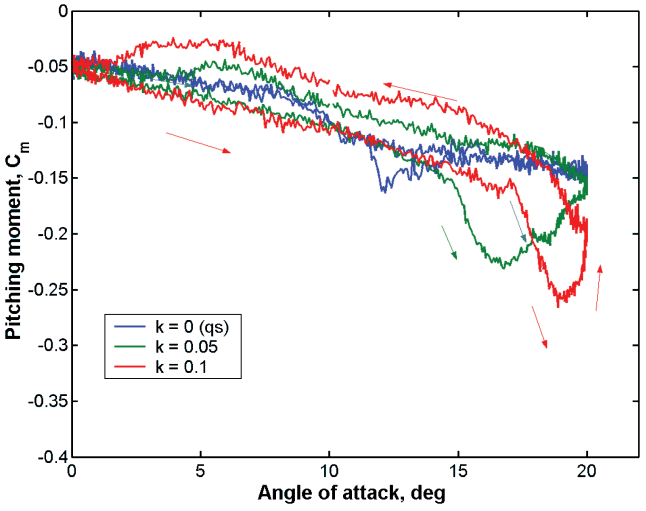

Fig. 14 Effect of reduced frequency on pitching-moment coefficient for the VDLE airfoil: $M = 0.3$, and $\alpha = 10$ deg +10 deg sin ωt.

also delayed for this case. Overall, for both $M = 0.3$ and 0.4 the results presented indicate that VDLE is effective in compressible dynamic stall control.

The pitching moments for the various cases under discussion are shown in Figs. 13 and 14 for $M = 0.3$. It is clear that for a basic VR-12 airfoil with no droop the pitching moment is strongly negative and exhibits the typical dynamic stall pitching-moment loop. The peak pitching moment drops with increasing droop; however, the value at $\alpha = 0$ deg increases steadily. Interestingly, the moment loop for $\delta = 20$ deg shows a fully anticlockwise loop, but, as has been discussed earlier, a fixed droop is undesirable for a rotor. In comparison, the VDLE case shows the most favorable pitching-moment variation, with a nearly zero value at $\alpha = 0$ deg and a peak value of about 40% of the basic case and a fully anticlockwise loop. Thus, there is only positive damping in this case, which implies that the negative effects of vortex convection are largely suppressed. In addition, this has a positive benefit in reducing the torsional vibrations of the rotor. It is seen from Fig. 14 that there is only nominal dependence of the pitching moment on reduced frequency k. The positive damping of the VDLE airfoil increases with k. At $M = 0.4$ (Fig. 15), similar results are obtained for the various cases considered. Thus, even though a simple droop might appear to be a way to reduce dynamic stall tendencies in a rotor the need to improve the advancing side performance and the general superiority of performance as seen in this study of the VDLE configuration makes it a worthwhile mode of operation.

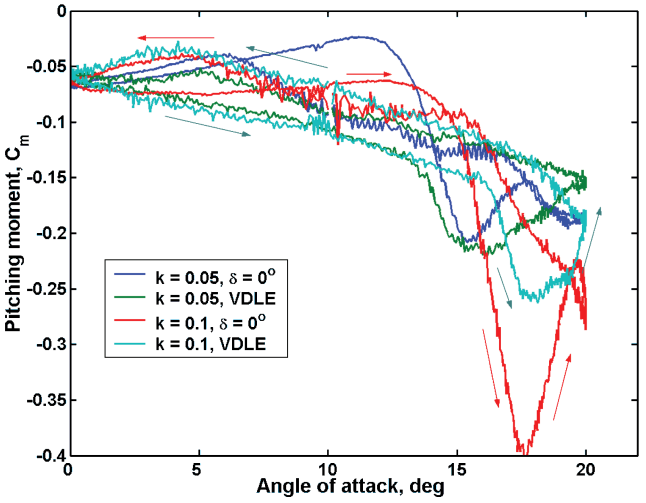

Fig. 15 Comparison of pitching-moment coefficient of the basic VR-12 airfoil and the VDLE airfoil: $M = 0.4$, and $\alpha = 10$ deg +10 deg sin ωt.

IV. Conclusions

A novel compressible dynamic stall control technique that uses a variably drooping leading edge airfoil was tested. Quantitative flow visualization and unsteady pressure measurements over an airfoil oscillating as $\alpha = 10$ deg $+10$ deg sin ωt were obtained for different Mach numbers, reduced frequencies, and airfoil droop configurations. The test cases included the basic VR-12 airfoil, the fixed-droop value of 5, 10, 15, and 20 deg and the VDLE airfoil. The results clearly demonstrated that the VDLE airfoil was effective in controlling compressible dynamic stall even when different stall onset mechanisms were involved. Dramatic differences in the flow evolution were seen for the various configurations. In particular, the flow over the leading edge was maintained below the critical value when the leading edge was drooped, thus reducing the adverse pressure gradient and mitigating both the compressibility effects and the dynamic stall process. Large reductions of drag and pitching-moment coefficients, ranging from 50 to 75%, were obtained, with acceptable lift performance, resulting an overall enhanced performance from the airfoil. The positive damping recorded for both $M = 0.3$ and 0.4 indicates that this concept is worthwhile to pursue for a rotor because it eliminates torsional instabilities in rotor harmonics, and thus a distinctly superior aeromechanical performance can be obtained under dynamic stall conditions of operation. This opens the possibility that the operational envelope of a rotor can be significantly extended.

Acknowledgments

This effort was initiated by the U.S. Army Aeroflight dynamics Directorate (AFDD) (C. Tung). Additional support was provided by the U.S. Army Research Office and monitored by T. L. Doligalski. This support through grants to the Naval Postgraduate School is gratefully acknowledged. The support of M. C. Wilder, NASA Ames Research Center in the development of the data-acquisition software for this work, the instrumentation support of AFDD, and the assistance of R. L. Miller, Sverdrup Technology, Inc., during the wind-tunnel studies are all sincerely acknowledged.

References

[1]Chandrasekhara, M. S., Wilder, M. C., and Carr, L. W., "On the Competing Mechanisms of Compressible Dynamic Stall," *AIAA Journal*, Vol. 36, No. 3, 1998, pp. 387–393; also AIAA Paper 96-1953, June 1996.

[2]Tung, C., and Chandrsekhara, M. S., "Review of Compressible Dynamic Stall Control Methods," *Proceedings of the AHS Heli- Japan Conference*, American Helicopter Society, Tochigi, Japan, Nov. 2002.

[3]Chandrasekhara, M. S., Wilder, M. C., and Carr, L. W., "Compressible Dynamic Stall Control Using Dynamic Shape Adaptation," *AIAA Journal*, Vol. 39, No. 10, 2001, pp. 2021–2024; also AIAA Paper 99-0655, Jan. 1999.

[4]Carr, L. W., Chandrasekhara, M. S., Wilder, M. C., and Noonan, K. W., "Effect of Compressibility on Suppression of Dynamic Stall Using a Slotted Airfoil," *Journal of Aircraft*, Vol. 38, No. 2, 2001, pp. 296–309; also AIAA Paper 98-0332, Jan. 1998.

[5]Yu, Y. H., Lee, S., McAlister, K. W., Tung, C., and Wang, C. M., "Dynamic Stall Control for Advanced Rotorcraft Application," *AIAA Journal*, Vol. 33, No. 2, 1995, pp. 289–295.

[6]Carr, L. W., and Chandrasekhara, M. S., "Design and Development of a Compressible Dynamic Stall Facility," *Journal of Aircraft*, Vol. 29, No. 3, 1992, pp. 314–318; also AIAA Paper-89-0647, Jan. 1989.

[7]Brock, N., Chandrasekhara, M. S., and Carr, L. W., "A Real Time Interferometry System for Unsteady Flow Measurements," *ICIASF'91 RECORD*, Inst. of Electrical and Electronics Engineers, New York, Oct. 1991, pp. 423–430.